applied sciences

MDPI

Article

Comparison of Electrochemically Deposited Bi and Sn Catalysts onto Gas Diffusion Electrodes for the Electrochemical CO_2 Reduction Reaction to Formate

Mila Manolova [1,*], Joachim Hildebrand [1,2], Sebastian Hertle [2], Şeniz Sörgel [1], Holger Kassner [1] and Elias Klemm [2]

[1] Department of Electrochemical Energy Systems, Research Institute for Precious Metals & Metals Chemistry (fem), Katharinenstrasse 17, 73525 Schwäbisch Gmünd, Germany; hildebrand@fem-online.de (J.H.); soergel@fem-online.de (Ş.S.); kassner@fem-online.de (H.K.)

[2] Institute of Technical Chemistry, University of Stuttgart, Pfaffenwaldring 55, 70569 Stuttgart, Germany; elias.klemm@itc.uni-stuttgart.de (E.K.)

* Correspondence: manolova@fem-online.de

Abstract: In this publication, we report about the selectivity and stability of bismuth (Bi)- and tin (Sn)-based electrocatalysts for the electrochemical CO_2 reduction reaction (eCO_2RR) for formate production. Bismuth and tin were successfully electrodeposited using the pulse plating technique on top of and inside of the gas diffusion layers (GDLs). The distribution of the catalyst throughout the thickness of the gas diffusion electrodes (GDEs) was investigated by using scanning electron microscopy and computer tomography; it was found that the catalyst morphology determines the performance of the electrode. Inhomogeneous deposits, with their enlarged catalyst surface area, provide more active centres for the eCO_2RR, resulting in increased Faraday efficiency (FE) for formate. The initial electrochemical characterisation tests of the bismuth- and tin-loaded GDEs were carried out under laboratory operating conditions at an industrially relevant current density of 200 mA·cm^{-2}; complete Sn dissolution with a subsequent deformation of the GDL was observed. In contrast to these results, no leaching of the electrodeposited Bi catalyst was observed. An FE of 94.2% towards formate was achieved on these electrodes. Electrodes based on an electrodeposited Bi catalyst on an in-house prepared GDL are stable after 23 h time-on-stream at 200 mA·cm^{-2} and have very good selectivity for formate.

Keywords: electrochemical deposition; Sn; Bi; gas diffusion electrodes (GDE); electrochemical CO_2 reduction reaction (eCO_2RR)

Citation: Manolova, M.; Hildebrand, J.; Hertle, S.; Sörgel, Ş.; Kassner, H.; Klemm, E. Comparison of Electrochemically Deposited Bi and Sn Catalysts onto Gas Diffusion Electrodes for the Electrochemical CO_2 Reduction Reaction to Formate. *Appl. Sci.* **2023**, *13*, 7471. https://doi.org/10.3390/app13137471

Academic Editor: Abdeltif Amrane

Received: 4 May 2023
Revised: 16 June 2023
Accepted: 21 June 2023
Published: 24 June 2023

1. Introduction

To achieve the global climate targets, the investigation of new technologies for a decarbonized energy production and storage method as well as defossilised chemical production method is inevitable. With the use of renewable electricity generated from solar or wind sources, CO_2 can be used as raw material for the electrochemical CO_2 reduction reaction (eCO_2RR) [1–5]. The electrochemical conversion of CO_2 into a diverse spectrum of chemicals is a potential technology to change the role of CO_2 from harmful waste to a valuable resource. Depending on the electrocatalyst, value-added products such as CO, formate/formic acid, alcohols, and other hydrocarbons can be produced from CO_2 by the eCO_2RR reaction [6–10].

Besides CO, formate/formic acid is an easily accessible product that can be used in various industrial applications and in downstream processes in the chemical industry [4,11,12]. The most common catalysts for the eCO_2RR reaction to formate/formic acid are based on tin (Sn) and bismuth (Bi). Both of these elements exhibit high selectivity towards formate/formic acid and high overpotentials towards the hydrogen evolution reaction [4,13–19]. Additionally, these catalysts are of interest because of their non-toxic properties and low cost [20].

To achieve industrially relevant current densities of 200 mA·cm^{-2} and greater, the use of gas diffusion electrodes (GDEs) is necessary [21,22]. State-of-the-art GDEs are fabricated by depositing a catalyst layer on a gas diffusion layer (GDL) [23,24]. This is typically performed by spray coating an ink [25–28] consisting of the catalyst, a binder, and a solvent onto the gas diffusion layer. Typically, to obtain the catalyst, the active phase (electrocatalyst) is deposited on a conducting support consisting of mainly carbon materials by a precipitation process [29].

Electrodeposition is a cost-effective and uncomplicated method that offers the possibility to selectively place catalyst particles at active positions of the triple-phase boundary [30]. Through a suitable choice of substrate, process, and electrolyte parameters, the nucleation rate and morphology of the precipitates can be influenced. As shown in the literature, defects, grain sizes, and orientation of the catalyst material that can be influenced in this way have a decisive influence on the selectivity and activity of the catalyst in the electrochemical CO_2 reduction [14–18,31–37]. Compared with the other techniques available, electrodeposition is the most straightforward method to fabricate large electrodes for real industrial electrolysers.

Aside from galvanostatic deposition, pulse current deposition (pulse plating, PP) is one of the most commonly techniques used in electrodeposition. It is known that the morphology, microstructure, hardness, ductility, porosity, and surface roughness of electrodeposits are impacted by the process parameters [20]. PP also yields a finer, homogeneous surface appearance because it is possible to achieve higher instantaneous current densities during electrodeposition.

In the literature, various metals (Sn, Bi, Pb, Hg, In) [13,21–27,29–33,38–41] have been investigated for the production of formate from CO_2 by electrolysis according to the following reaction:

$$CO_2 + H_2O + 2e^- \rightleftharpoons HCOO^- + OH^- \; E_0 = -0.72 \text{ V} \quad (1)$$

In most of the published papers, the catalyst precursors were deposited using the precipitation method, or the catalyst was used in the form of an ink. Some authors used electrodeposited catalysts on planar electrode substrates [15,42–49]. Only a few papers used GDEs/GDLs as the substrate for electrochemical deposition of Bi or Sn [50–52]. Usually, the electrodes have been investigated at low current densities [15,42–48] and short reaction times [15,43,45,47,49,52–54]. To clearly show the advantages of the electrochemical deposition, some of the results for Bi and Sn catalysts produced by different methods are compared in Table S1. There has been no study where the electrodeposited catalyst on GDE has been tested for long-term stability at the industrially relevant high current density of 200 mA·cm^{-2}.

In this work, Sn and Bi electrocatalysts were electrodeposited from commercial electrolytes using a pulse plating method on in-house fabricated and commercial carbon-based GDLs. The electrodes prepared in this way were investigated by using scanning electron microscopy and computer tomography before and after electrolysis. Different structures and morphologies of both electrocatalysts were electrodeposited on the surface and inside of the GDLs. The electrodes were electrochemically characterised at the high current density of 200 mA·cm^{-2} and the Faraday efficiency (FE) for formate was determined. The long-term stability (24 h) of the most promising electrodes was tested at industrially relevant current densities. The influence of the different coatings on the performance of the gas diffusion electrode concerning activity, selectivity, and stability in eCO_2RR was analysed. The catalytic performance (activity, selectivity, lifetime) of the electrodes was compared with GDEs that were produced via a precipitation method.

To achieve the high catalytic activity, selectivity, and long-term stability of the system, it is not only the catalyst selection, electrode materials and deposition techniques that are important. The choice of electrolyte [36,55–58], gas diffusion electrode design [22,23,29,34–37,59–65], and reactor design [4,66–74] can also influenced the CO_2RR reaction. The used cell design for the

electrochemical characterisation of the prepared electrodes has been described in previous work [29,36].

2. Materials and Methods

Chemicals: For the gas diffusion layers, 29 BC (SGL CARBON GmbH) (5% Polytetrafluoroethylene, areal weight 90 $g \cdot m^{-2}$, thickness: ca. 235 µm, el. resistance < 12 $m\Omega \cdot cm^{-2}$ [75]) and in-house (IH) fabricated gas diffusion layers were used; the latter items were prepared by mixing a carbon material (Acetylene Black, AB, Alfa Aesar, >99.9%) with polytetrafluoroethylene (PTFE, Dyneon, TF 92070Z, $\bar{d}p$ = 450 µm). For electrodeposition, commercial electrolytes supplied by Schloetter were used (Sn: Slototin MT 1110, conductivity 393 mS/cm; Bi: Slotoson MB 1880, pH 1, conductivity 314 mS/cm). The temperatures that were used were room temperature for Slototin MT 1110 and 45 °C for Slotoson MB 1880. For the anode, a Sn or Bi plate (Schloetter, 30 cm^2) was used. Potassium chloride (Carl Roth GmbH & Co KG, ≥99.5%), potassium bicarbonate (Carl Roth GmbH & Co KG, ≥99.9%), and potassium hydroxide (Carl Roth GmbH & Co KG, ≥85.0%) were used as conductive salts in the electrolyte for the electrochemical characterisation.

GDL preparation: The in-house fabricated GDLs were prepared using homogeneous mixing AB with PTFE at a ratio of 65:35 (30% PTFE) followed by dry-pressing at up to 7.29 $kN \cdot cm^{-2}$ for 4 min and a thermal treatment at 340 °C for 10 min in a nitrogen atmosphere [29]. In contrast to the thinner (235 µm) commercial GDL (Sigracet 29 BC carbon paper) used, for better stability, the in-house fabricated GDLs were thicker (thickness: ca. 900 µm). The two GDLs are schematically shown in Figure S1a,b.

Preparation of GDEs with precipitated electrocatalyst: GDEs with highly dispersed tin- or bismuth-based catalyst were used as the benchmarks for the GDEs with electrodeposited catalysts. First, the catalyst precursors were deposited using a pH-controlled precipitation method on acetylene black. Subsequently, the acetylene black with a deposited catalyst and the PTFE were mixed at a ratio of 65:35 followed by dry-pressing and thermal treating steps. The preparation method is described in detail in our previous work [34].

Preparation of GDEs with electrodeposited electrocatalyst (Scheme in Figure S1c): The electrochemical deposition experiments were conducted using a model SP-150 potentiostat/galvanostat (BioLogic) and were controlled using EC-Lab Software (BioLogic). The GDLs were coated using Sn electrolyte at room temperature (RT) and Bi electrolyte at 45 °C. In the PP experiments, square-wave pulses with cathode pulse current densities (j_p) of 5, 10, and 15 $A \cdot dm^{-2}$ and a pulse time (t_{on}) and relaxation time (t_{off}) of 1:1 s or 0.005:0.05 s (t_{on}/t_{off}), respectively, were used. The used current densities were recommended from the electrolyte producer, and the pulse and relaxation times were based on previous experience. The average current density j_{av} was calculated according to the following equation:

$$j_{av} = j_p \cdot t_{on}/(t_{on} + t_{off}) = j_p \cdot t_{on} \cdot f = j_p\ \theta \quad (2)$$

The duty cycle θ (θ = $t_{on}/(t_{on} + t_{off})$, %) and pulse frequency f (f = $1/(t_{on} + t_{off})$, Hz) for the used on-/off-times were θ = 50%, f = 0.5 Hz and θ = 9%, f = 18.18 Hz, respectively. These values were chosen according to previous experience and preliminary tests. The electrodeposited amounts of the different catalysts were kept constant by adjusting the deposition times. The reason for doing so is the nature of the GDL. For depositing inside of the GDL, the Bi electrolyte has to easily penetrate into the inside of the GDL. Both investigated GDLs were thick, and PTFE was part of their structure. The hydrophobic properties of PTFE are useful for the eCO_2RR reaction but complicate the penetration of an electrolyte into the inside of the GDL and complicate metal deposition. To enhance this process, the GDLs were pre-treated for 2 min in an ultrasonic bath of Sonorex (Bandelin electronics).

The used PP parameters are systemised in Table 1.

Table 1. Pulse plating parameters and their abbreviations.

Bi	Sn	$-j_{av}$, mA·cm^{-2}	$-j_{p}$, mA·cm^{-2}	t_{on}:t_{off}, s:s	θ, %	f, Hz	t, min
Bi-1-11-60	Sn-1-11-60	0.5	1	1:1	50	0.5	60
Bi-5-11-30	Sn-5-11-30	2.5	5	1:1	50	0.5	30
Bi-10-11-15	Sn-10-11-15	5	10	1:1	50	0.5	15
Bi-15-11-10	Sn-15-11-10	7.5	15	1:1	50	0.5	10
Bi-1-55-200	Sn-1-55-200	0.09	1	0.005:0.05	9	18.18	200
Bi-5-55-140	Sn-5-55-140	0.45	5	0.005:0.05	9	18.18	140
Bi-10-55-55	Sn-10-55-55	0.91	10	0.005:0.05	9	18.18	55
Bi-15-55-20	Sn-15-55-20	1.36	15	0.005:0.05	9	18.18	20

GDE characterisations: The surface morphology and chemical composition of the electrodeposits were determined using a high-resolution scanning electron microscope (SEM, Gemini SEM 300, Zeiss) with energy dispersive X-ray spectroscopy (EDX) operated at 15 kV. Computer tomography (CT) cross-sections of the GDEs were performed using a Phoenix VtomexL 450 system (GE Sensing & Inspection Technologies). The phase analysis was performed by using X-ray diffraction in the Bragg–Brentano geometry using a D8 discover Da Vinci diffractometer (Bruker AXS GmbH, Karlsruhe, Germany) equipped with a 1D Lynxeye-XET detector using copper radiation. A variable divergence slit with an opening of 10 mm was used to keep the radiated area of the sample constant during the measurement. The phase analysis was performed by comparing the measured reflections to the ICDD-PDF2 database (International Centre for Diffraction Data). The roughness of the electrodes was investigated using the Nanofocus µsurf custom, (NanoFocus AG, Germany). The evaluation of the data was carried out using the software "Digital Surf MountainsMap® 7.2".

Electrochemical characterisation: The electrochemical characterisation of the prepared electrodes was performed in a custom-made semi-batch cell constructed from poly(methyl methacrylate) (PMMA). The used cell design was described in a previous work [29]. For the reaction condition, the conditions optimized by Löwe et al. were used as a starting point [36]. For experiments with reaction times (time on stream, TOS) > 1 h, the cell was modified for a continuous exchange of the electrolyte. The electrodes were separated by a cation exchange membrane (Nafion® 117, DuPont). The experiments were conducted using a Gamry Inferface 1010E potentiostat.

For GDEs coated with Sn, 1 M of $KHCO_3$ with a pH value of 10 was used as the electrolyte. Hg/HgO (1 mol/L KOH) served as the reference electrode. A platinum wire was used as the counter electrode. The electrolyte was heated and monitored by an external heat exchanger. On the gas side, a nickel mesh was used as a current collector. To protect the GDE from mechanical destruction by the nickel mesh, a GDL (SGL, Sigracet GDL 35AA) was placed between the mesh and the GDE. For Bi-based catalysts, to avoid the formation of carbonate and bicarbonate in the GDL, 1 M of KCl (pH 10) was used as a catholyte. The other materials and parameters remained the same. For the electrochemical characterisation, the geometrical area of the GDE was limited to 1 cm^2 by a PTFE mask. The characterisation was carried out at 50 °C and a CO_2 flow rate of 5.57 mL·min^{-1}. These conditions have been shown to be the optimum scenario in a similar system in a previous work [29]. The FE was calculated according to Equation (3) [36]:

$$\mathrm{FE} = \frac{n \cdot t \cdot I}{z \cdot F} \tag{3}$$

where n is the amount of substance (mol), t is the time (s), I is the current (A), z is the number of transferred electrons, and F is the Faraday constant (C·mol^{-1}).

All FE values presented in the manuscript are the average values from 3 different electrodes prepared in the same way.

To characterise the GDE, the current was increased in 60 s from 0 mA·cm^{-2} to −200 mA·cm^{-2} as preconditioning. This was followed by a galvanostatic hold for 1 h at −200 mA·cm^{-2}. Long-term experiments over 24 h were performed at a current density of −200 mA·cm^{-2} and −50 mA·cm^{-2}. The electrolyte was continuously exchanged at a flow rate of 1 mL·min^{-1}. The gaseous products (H_2, CO) were analysed using a thermal mass flow meter and online GC (Agilent 7890A). To quantify the formate concentration, a high-performance liquid chromatography (HPLC, Agilent Technology, 1260 Infinity, column: NUCLEOGEL Sugar 810 H) analysis was performed.

3. Results and Discussion

3.1. Bi PP Electrodes Based on In-House GDLs

The performance of the Bi-IH-PP-GDLs for formate production highly depends on the used PP parameters, such as the cathodic pulse current density j_p, pulse time t_{on}, and relaxation time t_{off}. (Figure 1a). The PP parameters had an effect on the surface morphology of the deposited Bi, which determines the FE for the formate production. Decreasing j_p with a t_{on}:t_{off} of 1:1 led to an increase in the electrode performance from approx. 10% to approx. 90% (white bars in Figure 1a). The deposition time was calculated such that coatings of an equal thickness of 5 µm were deposited. At j_p = −15 A·dm^{-2} and t_{on}:t_{off} = 1s:1s, a compact Bi deposit with crystallites of over 5 µm, which were separated from each other through a few grain boundaries, were electrodeposited on the GDL (Figure 1b). The CT cross-section image shows that the Bi deposit is only located on the top of the GDL (Figure 1d). With the decrease in PP current density, the size of the crystallites decreases (Figure S2a). Small current densities (j_p = −5 A·dm^{-2}) lead to the growth of more nuclei on the GDL. The resulting Bi deposit is coarse-grained with crystallites of up to 2 µm (Figure S2b), and it is rich in different defects. This enhances the CO_2 diffusion through the catalyst layer. As a result, the FE for formate reaches its maximum value (Figure 2a, white bars, 5 A·dm^{-2}). The potentials of the electrodes are shown in Table S2.

The effect of a short deposition time t_{on} in combination with longer pause time t_{off} on the morphology and electrode performance, respectively, is especially visible at high current densities. The Bi deposit at t_{on}:t_{off} = 1 s:1 s is compact, only being located on the top of the GDL (Figure 1b,d) and having only reached a 10% FE for formate (Figure 1a white bar, j_p = −15 A·dm^{-2}). On the surface of Bi-IH-PP deposited at the same j_p but with t_{on}:t_{off} = 0.005 s:0.05 s, an increased number of single Bi crystallites and their aggregates randomly grew. This inhomogeneous structure, which is rich in sharp edges, grain boundaries, and other defects, provides an enlarged active surface area. Moreover, the CT cross-section image of the same GDE shows that at t_{on}:t_{off} = 0.005 s:0.05 s, the growth of inhomogeneous insular structures occur not only on the top of the GDE electrode, but also inside of the GDE up to a 170 µm depth (Figure 1e). During CO_2 electrolysis, the wetted area as well as the reaction zone moves towards the gas side of the GDL used [76,77]. According to this information, to achieve better electrode performance, the catalyst grains or particles should be evenly distributed not only on the top of the GDL but also inside of the GDL. Due to the reduction of mass transport limitations of CO_2 and liquid products, such a catalyst distribution can improve the FE to 90% (Figure 1a, hatched bar, j_p = −15 A·dm^{-2}). At this t_{on}:t_{off}, Bi was also deposited inside of the GDLs independent of the used current density (Figure S2c).

The catalyst roughness also influences the FE of the GDEs. A homogeneous Bi catalyst (Bi-15-11-10) with area roughness parameters (Sa) of 1.55 µm has a low FE for formate (10%). Bi deposits with inhomogeneous insular structures (Bi-5-55-140, Figure S1c) with an almost fourfold increase in the Sa of 5.57 µm (Figure S3) reached a greater than 90% FE for formate (Figure 1a).

After CO_2 electrolysis, the Bi deposit remains on the top and also inside of the GDL (Figure 2a); however it remains with a structure that has changed (Figure 2b). The Bi crystallites are converted independent of the electrolysis parameters into sharp plates (scales) with enormous surface area (Figure 2b). The EDX spectra show a high amount of

oxygen (Figure S4). We suppose that the Bi catalyst was oxidized during the CO_2 reduction reaction; this did not change the FE of the electrode, because it is well-known from the literature that Bi-based catalysts are active in oxide and reduced metal forms [50,77,78].

During PP deposition with short deposition time and longer pauses (t_{on}:t_{off} = 0.005 s:0.05 s), thin channels were formed inside of the Bi deposit (Figure 2c). Thus, an increase in the active surface area was achieved. The electrolyte wets and CO_2 diffuses are facilitated through the channels inside of the Bi electrocatalyst, and the aimed synergetic effect between catalyst and GDL properties is achieved. As a result, the FE for formate for Bi-IH-PP GDE reaches 93% (Figure 2a).

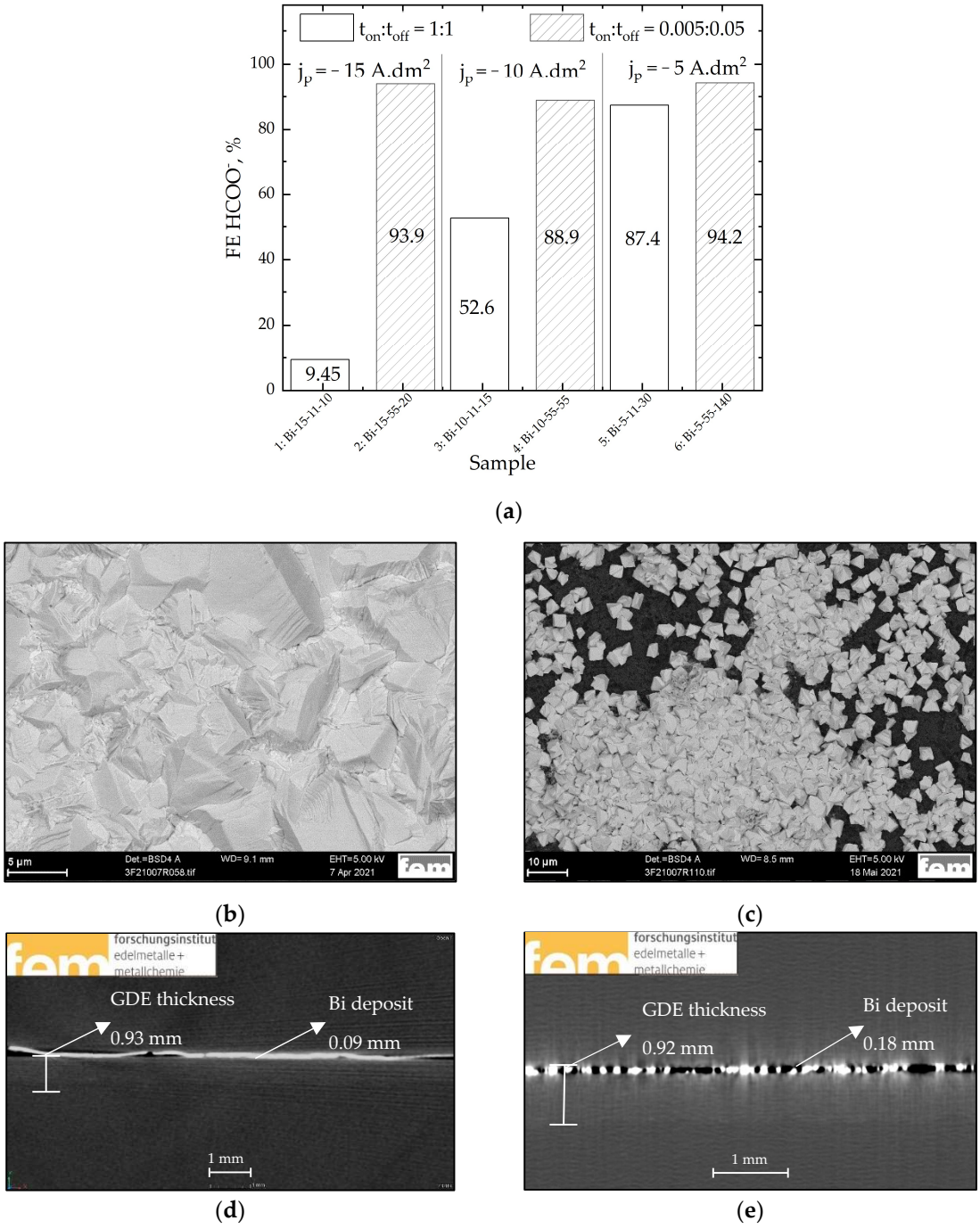

Figure 1. Investigations of Bi-IH-PP GDEs. (**a**) Effect of PP parameters on the FE for formate. Tested at 200 mA·cm^{-2}, 50 °C, 60 min; (**b**) SEM image from the surface of Bi-15-11-10 GDE; (**c**) SEM image of Bi-15-55-20 GDE; (**d**) CT cross-section of Bi-15-11-10 GDE; (**e**) CT cross-section of Bi-15-55-20 GDE.

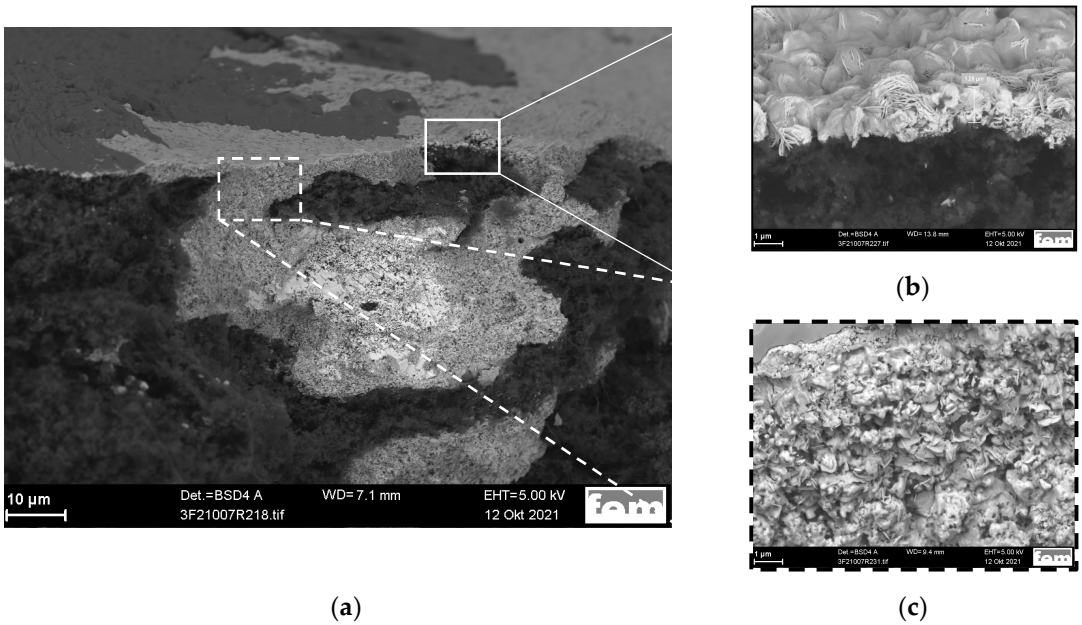

Figure 2. Bi-IH-PP GDE Bi-5-55-140 after CO_2 electrolysis at 200 mA·cm^{-2}, 50 °C, 60 min: (**a**) SEM cross-section image; (**b**) enlargement of the active surface by Bi deposited on top of the GDL; and (**c**) enlargement of the active surface by Bi deposited inside of the GDL.

The Bi-IH-PP GDEs that showed the best results during the shorter eCO_2RR (Figure 1a) were tested for the long-term CO_2 electrolysis. It is supposed that the most possible reason for this very good performance of the PP electrode is the uneven distribution of the Bi catalyst (see Figure 1c,e) on top of and also inside of the GDL. The FE of formate for all tested Bi-IH-PP electrodes (long-term tests) was greater than 80%, and in some cases, it reached 94%. It was found that the FE was dependent on the GDL that was used. The reproducibility in one GDL batch was 95–100%. However, there were observed distinctions between different batches. Freshly produced GDLs after Bi deposition reached an FE of greater than 94% (Figure 1a). Older batches showed a lower FE because the deposited Bi amount was lower. Egetenmeyer et al. [79] showed that the laser surface etching of GDL before the electrodeposition of Pt enhanced the electrochemical deposition. Most likely, the in-house prepared substrates achieved different aging stages because of time, which only affects the electrochemical deposition. The carried out electrochemical measurements (CV, galvanostatic experiments) of the blank GDL did not show any changes; therefore, in Figure 3, the electrode with the best performance is not shown. The benchmark electrode Bi-IH-P with the fine catalyst distribution is still better (Figure 3) than the Bi-IH-PP electrodes. The electron balance for electrodes with an electrodeposited catalyst is sometimes not closed. In the used setup, the produced hydrogen typically diffuses through the porous GDL towards the gas side of the electrode; it is there that hydrogen, other gaseous products, and non-converted CO_2 are detected. Due to the Bi that was deposited on top of the GDE, some H_2 was released into the electrolyte on the cathode side, which could be observed as gas bubbles in the electrolyte. A detection of gases at the electrolyte side of the GDL was not possible in the setup used. As a result, the missing FE can be dedicated to H_2. A small increase in the HER at TOS > 15 h was observed. After a reaction time of 23 h at these high current densities (200 mA·cm^{-2}), the FE for formate was still 76.4%. The loss on selectivity and the small increase in the HER are not related to a degradation of the Bi catalyst. It is supposed that the growth of sharp plates of oxidized Bi and the restructuring of the last Bi atomic layer mechanically deformed the GDL structure. The optimized relation between the distribution of electrodeposited Bi and the GDL stability must be thoroughly investigated. Through this analysis, it should be possible to fabricate functioning GDEs

over a long period of time, which is required for an industrial application of these electrodes. The potentials of the electrodes are shown in Figure S5.

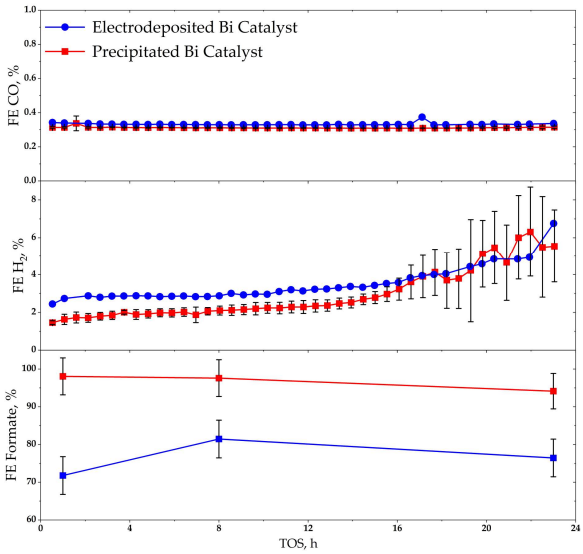

Figure 3. Product contribution of Bi-IH-PP GDE, Bi-5-55-140 (dots) with Bi-IH-P GDE (squares). Tested at 200 mA·cm^{-2}, 50 °C, 24 h.

3.2. Bi PP Electrodes Based on 29 BC GDLs

In order to prove if a commercial GDL provides similarly good electrodes when using a PP method to deposit Bi, a 29 BC gas diffusion layer from SGL Carbon was chosen. The BC GDL was thinner (230 µm) and had a structure and composition that was different than the IH GDL. Using SEM images, it was possible to distinguish the different layers of the BC GDL. Using CT imaging, the well-ordered pore structure of the different layers can be seen [30]. After Bi PP depositon, coarse-grained Bi deposits were placed not only on top of the BC but also inside of the microporous layer (Figure 4a). In the middle of the GDL BC, Bi was homogeneously deposited, preserving the well-ordered pore structure (Figure 4b). Bi was deposited into the whole GDL layer down to the backside of it at 190 µm.

In agreement with the investigations on the IH GDL with Bi, no Bi dissolution on the top or inside of the GDL was observed (Figure 4c). The FE reached for formate for 1 h in a Bi-BC-PP electrode was 80%, which is at least 10% lower compared with the Bi-IH-PP and Bi-IH-P GDEs (Figure S6). Until now, it was not possible to achieve a higher FE for formate.

After 24 h of operation at 50 mA·cm^{-2}, only the Bi crystallites transformed into sharp plates (scales) with a higher surface area (inset of Figure 4c). This is in accordance with our results for Bi-IH-PP GDE (see Figure 1b). XRD measurements revealed that the main phase after 24 h of CO_2 electrolysis was metallic Bi with a preferred <012> orientation normal to the sample surface. Regarding the intermediate phase, bismutite carbonate ($Bi_2(CO_3)O_2$) was found. Some reflections with low intensity indicated the presence of potassium bismuth oxide ($KBi_{12}O_{18}$) in traces (Figure S7). According to the Pourbaix diagram of Bi, under reaction conditions (−1.43 V vs. SHE, pH > 10), the thermodynamically stable Bi species is elementary Bi [80]. The selectivity of the tested Bi-PP-BC electrode did not change with time. The reason for this could be that there is no difference in the reactivity of the metallic Bi phase and Bi oxides in the eCO_2RR reaction towards formate [42]. After eCO_2RR, the texture of the GDL remained unchanged. This is at odds with our previous research for the Sn catalyst, where the GDL texture was completely destroyed after 1 h of electrolysis [30]. The observed black spots (blemishes) in Figure 4d are only mechanical deformations that are caused by the electrolysis process.

The Bi-BC-PP GDE were also tested for their long-term stability at a higher current density of 200 mA·cm^{-2}. However, the mechanical stability of the GDE based

on the commercial GDL was not good enough, and after 10 h, the Bi-BC-PP GDE was mechanically destroyed.

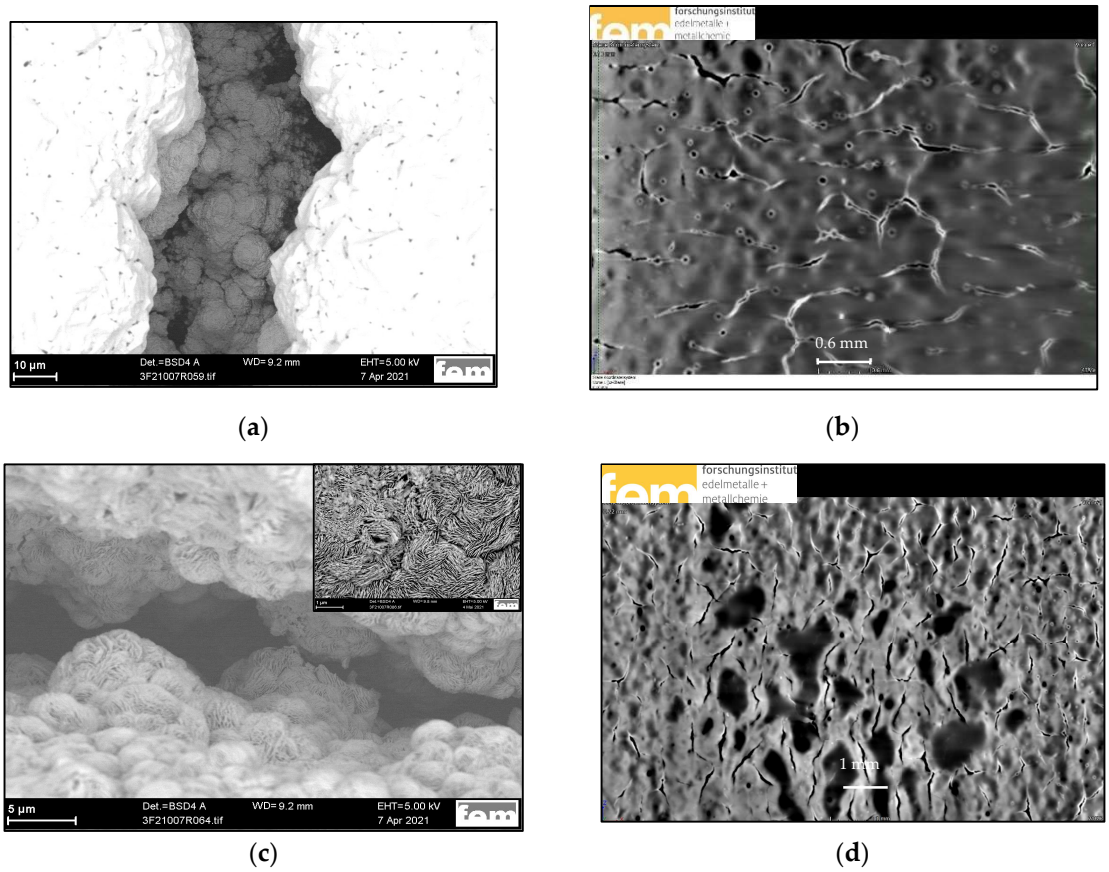

Figure 4. Bi-BC-PP GDE Bi-15-11-10 before eCO_2RR: (**a**) SEM image with surface morphology on top of the GDL and on the next microporous layer; (**b**) CT scan in the middle of the sample. Bi-BC-PP GDE Bi-15-11-10 after eCO_2RR (50 mA·cm^{-2}, 50 °C, 24 h): (**c**) SEM image, surface morphology inside of the GDL. Inset with surface morphology on top of the GDL; (**d**) CT scan inside of the GDE.

Due to a different structure and composition, the in-house fabricated GDLs are more suitable as substrates for catalysts constructed via electrodeposition compared with the chosen commercial GDLs. With the further optimisation of the structure and composition of GDLs, an optimized electrodeposition of catalysts, and a good understanding of the processes during electrolysis, the long-term stable operation of Bi-GDEs fabricated by the pulse plating technique should be achieved.

3.3. Sn PP Electrodes Based on In-House GDLs

In our previous work [30], Sn electrodeposition was demonstrated on the top of and inside of the commercial GDL 29 BC. The highest FE for formate that was attained with such GDEs was 85%. In this work, in order to increase the Faraday efficiency for formate as well as the electrode stability for the Sn electrodeposition, the optimized in-house fabricated electrode [37] was used.

Coarse-grained Sn coatings with intergrown crystallites ranging from 0.5 µm to 2 µm were deposited on the top of IH fabricated GDL by PP at $j_p = -1$ A·dm^{-2} and t_{on}:t_{off} = 1 s:1 s (Figure 5a). At a shorter t_{on}:t_{off} time, single coarse-grained crystallites (1 µm) with sharp edges grew on the GDL surface (Figure 5b). The crystallites were separated from each other through hollows or were grouped into islands. Additionally, unevenly distributed small crystallites with a size of about 0.1 µm were deposited on top of them; some of them are marked with red circles in Figure 5b. It is supposed that such an inhomogeneous surface

morphology of the electrodeposited catalyst additionally enlarges the active surface area and will lead to an increased FE of the GDE.

The Sn-IH-PP GDEs were thoroughly investigated in the CO_2 electrolysis. As a benchmark, state-of-the-art Sn-IH-P GDEs were used [36,37]. In accordance with the Bi-IH-PP GDEs, it was found that the surface morphology of the electrodeposited Sn coating has an influence on the FE for formate and on the product distribution (Figure 5c). The more compact deposit (Figure 5a), where CO_2 mainly penetrated through the grain boundaries and other deposit defects, showed a lower selectivity for formate (FE: 82.3%) than the inhomogeneous deposit (FE: 93.1%) (Figure 5b), where CO_2 additionally penetrated through the enlarged catalyst surface (an increased number of sharp edges) and free spaces between the crystallite islands. On the GDL with the pulse plated electrocatalyst with shorter t_{on}:t_{off} time, the FE for formate (93.1%) was even better than that of the Sn-IH-P electrodes (87.1%, Figure 5c, last column). The Sn content of both electrodes (Figure 5c) was comparable (2.6 wt.% Sn on GDEs with precipitated catalyst, 3.7 wt.% Sn on GDEs with electrodeposited catalyst). These electrodes feature a low selectivity for the side products of CO (12%) and H_2 (1%), as shown in our previous publication [30]. The potentials of the electrodes are shown in Table S3.

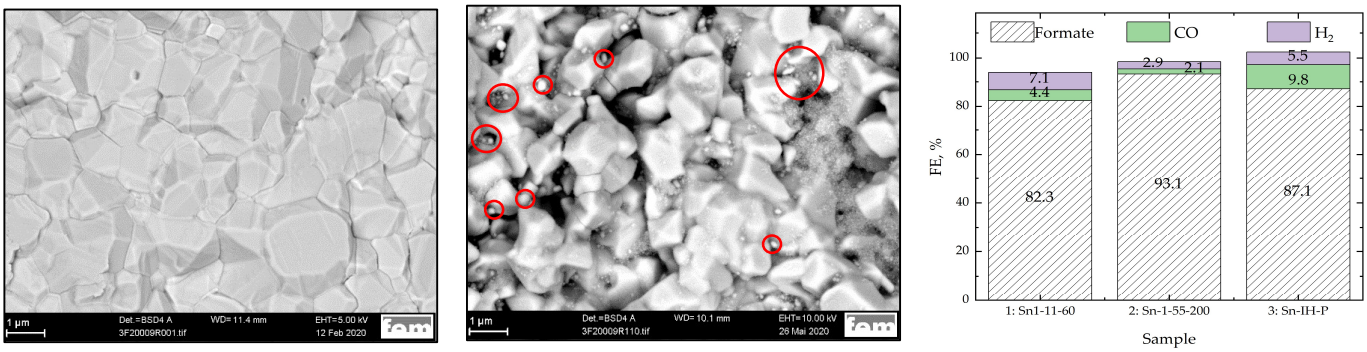

(**a**) (**b**) (**c**)

Figure 5. Investigations of Sn-IH-PP GDE. (**a**) SEM images of Sn-1-11-60; (**b**) SEM images of Sn-1-55-200; (**c**) FE for formate and product distribution for the electrodes with electrodeposited catalysts Sn-1-11-60 and Sn-1-55-200, as well as an electrode with a precipitated Sn catalyst. Electrochemical tests conditions: 200 mA·cm^{-2}, 50 °C; time on stream (TOS): 60 min.

The long-term electrolysis for Sn-IH-PP GDE was carried out at 50 mA·cm^{-2} because when applying a current density of 200 mA·cm^{-2}, the HER increases after two hours, wherein no stable reaction would be possible after this time. In the beginning of the electrolysis, the FE was at about 97% and was quite stable for 4 h (Figure 6). Then, the selectivity for formate decreased to approximately 90% and was almost stable for another 6 h. The FE for hydrogen evolution reaction at this time was under 2%. After 11 h, the FE for formate decreased in a step-by-step manner. Simultaneously, the HER as a competing reaction became more favoured. This could indicate the leaching of the active catalyst. Furthermore, leaching of a SnO_X catalyst prepared by the precipitation method has been reported [34,67]. After 18 h, the main reaction was that the HER and experiment was interrupted.

The same Sn-IH-PP GDE was investigated using CT imaging before and after the long-term electrolysis. The Sn catalyst was only deposited on the surface of the IH-GDL (Figure 7a). After 19 h of CO_2 electrolysis at 50 mA·cm^{-2}, the Sn catalyst layer on top of the sample was completely dissolved, large agglomerates were found inside of the GDL, and the GDL thickness increased from 0.9 mm to 1.4 mm (Figure 7b). In the SEM image (Figure 5c), the dark grey areas represent the GDL (Spectra 6, Figure S8a). EDX measurements in some lighter areas on the surface and inside of the GDL (Spectra 5, Figure S8b) revealed the presence of large amounts of K and O. During the long-term

electrolysis, secondary products such as carbonates or bicarbonates were formed in a non-Faradaic side reaction at high pH values in the pore systems of the used electrodes. These carbonate salts precipitated inside the GDL and increased its thickness through the process of swelling. Bienen et al. [34] also observed SnO_2 leaching from the same in-house fabricated GDL, where the Sn catalyst was not electrochemically deposited but instead had Sn particles finely deposited on the carbon black via a homogeneous precipitation method with urea. According to the Pourbaix diagram of Sn [80], metallic Sn is the thermodynamically stable phase at these potentials at a pH value of at least 10. It must be mentioned that due to the generated OH^- ions during the ongoing reactions of eCO_2RR and HER, the pH value inside the GDL can significantly exceed the value of 10 [66]. It seems that at such high pH values, and due to the negative potential, the metallic Sn is not stable. Sn dissolves, and over time, less catalyst is available in the deposited layer of the Sn electrocatalyst. Finally, no catalyst remains on the surface (see Figure 7b,c).

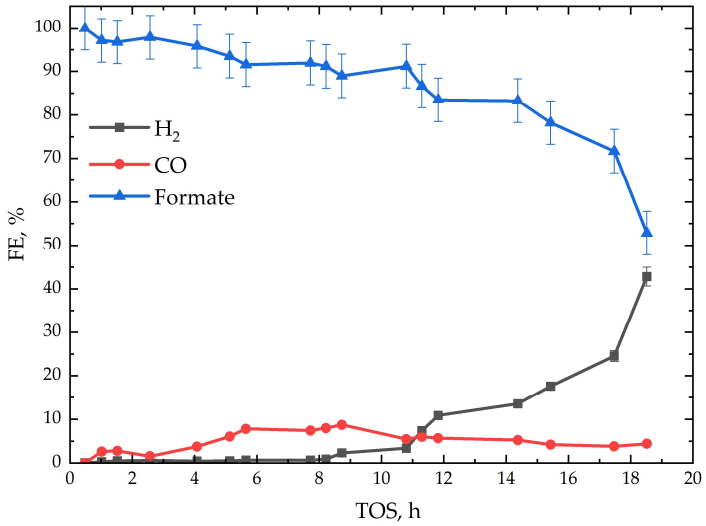

Figure 6. Product distribution of the Sn-IH-PP GDE, Sn-1-11-60. Electrochemical tests conditions: 50 mA·cm^{-2}, 50 °C, 19 h.

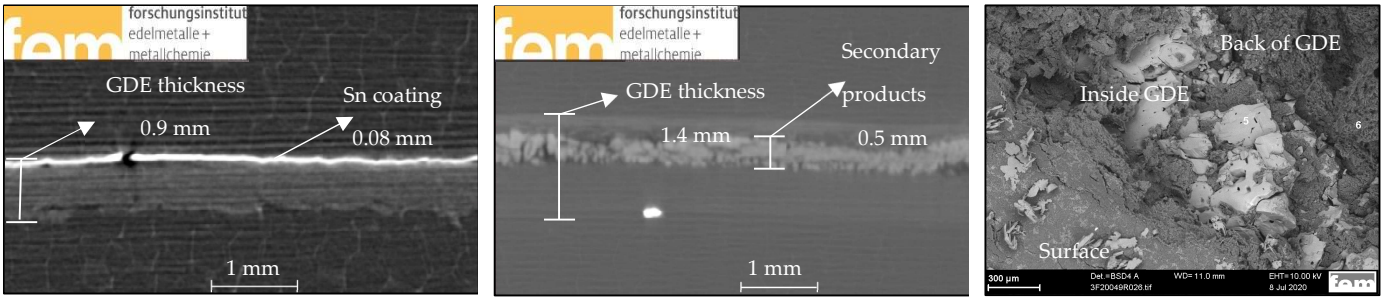

Figure 7. Sn-IH-PP GDE, Sn-1-11-60: (**a**) CT cross-section of Sn-IH-PP-GDE before electrolysis; (**b**) CT cross-section of the Sn-IH-PP-GDE after 19 h of electrolysis; (**c**) SEM cross-section of the electrode after 19 h of electrolysis at 50 mA·cm^{-2} at 50 °C with the secondary products inside the GDL.

To summarise, these results indicate that Sn is not stable as a catalyst for eCO_2RR at high current densities. Locally high pH values undoubtedly cause the dissolution of Sn. This can be unambiguously concluded to be due to the complete dissolution of the electrodeposited Sn layer at these conditions.

4. Conclusions

Sn and Bi catalysts were successfully electrodeposited using the pulse plating method on top of and inside of the commercial and in-house fabricated GDLs.

The electrodes were tested in an electrolysis cell at industrially relevant current densities up to 200 $mA \cdot cm^{-2}$.

It was found that the catalyst morphology determines the performance of the electrode. Inhomogeneous deposits provide more active centres for the CO_2 reduction reaction, resulting in an increased FE for formate.

Upon CO_2 electrolysis at high current densities, complete dissolution of the electrodeposited Sn catalyst was observed. Furthermore, carbonate and bicarbonate formation was found inside of the GDLs.

No leaching of the electrochemically deposited Bi catalyst on the in-house fabricated GDLs was observed during CO_2 electrolysis at high current densities. An FE of 94.2% towards formate was achieved in these electrodes.

Such electrodes also have promising long-term stability (23 h) for the eCO_2RR at industrially relevant current densities (200 $mA \cdot cm^{-2}$) and have a very good selectivity for formate.

Supplementary Materials: The following supporting information can be downloaded at https://www.mdpi.com/article/10.3390/app13137471/s1: Figure S1: Investigations of Bi-IH-PP GDEs. (a) SEM image of Bi-IH-PP, Bi-10-11-15; (b) SEM image of Bi-IH-PP, Bi-5-11-30; (c) CT image of Bi-IH-PP, Bi-5-55-140. Table S1: Potentials of the electrodes shown in Figure 1a–c. Table S2: Potentials of the electrodes shown in Figure 4 (1–6). Table S3: Potentials of the electrodes shown in Figure 5a–c. Figure S2: EDX-spectra of Bi-IH-PP, Bi-5-55-140 GDE after eCO_2RR at 200 $mA \cdot cm^{-2}$, 50 °C, 60 min. Figure S3: (a) Spectra 6 and (b) Spectra 5. Figure S4: Potentials of Figure 6. Potentials of Bi-IH-PP GDE, Bi-5-55-140 (blue) with Bi-IH-P GDE (red). Tested at 200 $mA \cdot cm^{-2}$, 50 °C, 24 h. Figure S5: The FE for formate and product distribution for electrodes with electrodeposited catalysts Bi-BC-PP (15-11-10), shown in column (a); the electrodeposited catalysts Bi-IH-PP (15-55-20), shown in column (b); and an electrode with a precipitated Bi catalyst, shown in column (c). Electrochemical tests conditions: 200 $mA \cdot cm^{-2}$, 50 °C, time on stream (TOS): 60 min. Figure S6: XRD measurements of Bi-BC-PP GDE Bi-15-11-10 after eCO_2RR (50 $mA \cdot cm^{-2}$, 50 °C, 24 h). Figure S7. XRD measurements of Bi-BC-PP GDE Bi-15-11-10 after eCO2RR (50 $mA \cdot cm^{-2}$, 50 °C, 24 h). Figure S8. (a) GDL (Spectra 6); (b) GDL (Spectra 5).

Author Contributions: Conceptualization, E.K. and Ş.S.; investigation, M.M., J.H. and S.H.; writing—original draft preparation, M.M. and J.H., writing—review and editing, Ş.S. and E.K.; supervision, E.K. and H.K.; project administration, M.M. All authors have read and agreed to the published version of the manuscript.

Funding: This research was funded by the German Federal Ministry for Economic Affairs and Climate Action under grant number AiF/IGF 47 EWN.

Institutional Review Board Statement: This study did not require ethical approval.

Informed Consent Statement: Not applicable.

Data Availability Statement: Not applicable.

Acknowledgments: The authors thank Reinhard Böck, who provided review and editing assistance during the composition of the manuscript.

Conflicts of Interest: The authors declare no conflict of interest. The funders had no role in the design of the study; in the collection, analyses, or interpretation of data; in the writing of the manuscript; or in the decision to publish the results.

Abbreviations

BC	Commercial 29 BC GDL
IH	In-house prepared GDL
PP	Pulse plating
ED	Electrodeposition
P	Precipitation
NS	Nanostructure
NP	Nanoparticles
For GDEs:	
Bi-BC-PP	Bi deposited on a commercial GDL via pulse plating
Bi-IH-PP	Bi deposited on an in-house fabricated GDL via pulse plating
Bi-IH-P	Bi deposited on an in-house fabricated GDL via precipitation
Sn-BC-PP	Sn deposited on a commercial GDL via pulse plating
Sn-IH-PP	Sn deposited on an in-house fabricated GDL via pulse plating
Sn-IH-P	Sn deposited on an in-house fabricated GDL via precipitation

References

1. De Luna, P.; Hahn, C.; Higgins, D.; Jaffer, S.A.; Jaramillo, T.F.; Sargent, E.H. What Would It Take for Renewably Powered Electrosynthesis to Displace Petrochemical Processes? *Science* **2019**, *364*, eaav3506. [CrossRef]
2. Abanades, J.C.; Rubin, E.S.; Mazzotti, M.; Herzog, H.J. On the Climate Change Mitigation Potential of CO_2 Conversion to Fuels. *Energy Environ. Sci.* **2017**, *10*, 2491–2499. [CrossRef]
3. Jouny, M.; Luc, W.; Jiao, F. General Techno-Economic Analysis of CO2 Electrolysis Systems. *Ind. Eng. Chem. Res.* **2018**, *57*, 2165–2177. [CrossRef]
4. Fernández-Caso, K.; Díaz-Sainz, G.; Alvarez-Guerra, M.; Irabien, A. Electroreduction of CO_2: Advances in the Continuous Production of Formic Acid and Formate. *ACS Energy Lett.* **2023**, *8*, 1992–2024. [CrossRef]
5. Aldaco, R.; Butnar, I.; Margallo, M.; Laso, J.; Rumayor, M.; Dominguez-Ramos, A.; Irabien, A.; Dodds, P.E. Bringing Value to the Chemical Industry from Capture, Storage and Use of CO_2: A Dynamic LCA of Formic Acid Production. *Sci. Total Environ.* **2019**, *663*, 738–753. [CrossRef]
6. Saravanan, A.; Senthil Kumar, P.; Vo, D.V.N.; Jeevanantham, S.; Bhuvaneswari, V.; Anantha Narayanan, V.; Yaashikaa, P.R.; Swetha, S.; Reshma, B. A Comprehensive Review on Different Approaches for CO_2 Utilization and Conversion Pathways. *Chem. Eng. Sci.* **2021**, *236*, 116515. [CrossRef]
7. Jhong, H.R.M.; Ma, S.; Kenis, P.J. Electrochemical Conversion of CO_2 to Useful Chemicals: Current Status, Remaining Challenges, and Future Opportunities. *Curr. Opin. Chem. Eng.* **2013**, *2*, 191–199. [CrossRef]
8. Gao, D.; Arán-Ais, R.M.; Jeon, H.S.; Roldan Cuenya, B. Rational Catalyst and Electrolyte Design for CO_2 Electroreduction towards Multicarbon Products. *Nat. Catal.* **2019**, *2*, 198–210. [CrossRef]
9. Rumayor, M.; Dominguez-Ramos, A.; Perez, P.; Irabien, A. A Techno-Economic Evaluation Approach to the Electrochemical Reduction of CO_2 for Formic Acid Manufacture. *J. CO2 Util.* **2019**, *34*, 490–499. [CrossRef]
10. Rumayor, M.; Dominguez-Ramos, A.; Irabien, A. Formic Acid Manufacture: Carbon Dioxide Utilization Alternatives. *Appl. Sci.* **2018**, *8*, 914. [CrossRef]
11. Agarwal, A.S.; Zhai, Y.; Hill, D.; Sridhar, N. The Electrochemical Reduction of Carbon Dioxide to Formate/Formic Acid: Engineering and Economic Feasibility. *ChemSusChem* **2011**, *4*, 1301–1310. [CrossRef] [PubMed]
12. Kim, H.-Y.; Choi, I.; Ahn, S.H.; Hwang, S.J.; Yoo, S.J.; Han, J.; Kim, J.; Park, H.; Jang, J.H.; Kim, S.-K. Analysis on the Effect of Operating Conditions on Electrochemical Conversion of Carbon Dioxide to Formic Acid. *Int. J. Hydrogen Energy* **2014**, *39*, 16506–16512. [CrossRef]
13. Yang, Z.; Oropeza, F.E.; Zhang, K.H.L. P-Block Metal-Based (Sn, In, Bi, Pb) Electrocatalysts for Selective Reduction of CO_2 to Formate. *APL Mater.* **2020**, *8*, 060901. [CrossRef]
14. Han, N.; Wang, Y.; Yang, H.; Deng, J.; Wu, J.; Li, Y.; Li, Y. Ultrathin Bismuth Nanosheets from in Situ Topotactic Transformation for Selective Electrocatalytic CO_2 Reduction to Formate. *Nat. Commun.* **2018**, *9*, 1320. [CrossRef] [PubMed]
15. Su, P.; Xu, W.; Qiu, Y.; Zhang, T.; Li, X.; Zhang, H. Ultrathin Bismuth Nanosheets as a Highly Efficient CO_2 Reduction Electrocatalyst. *ChemSusChem* **2018**, *11*, 848–853. [CrossRef]
16. Qiu, Y.; Du, J.; Dai, C.; Dong, W.; Tao, C. Bismuth Nano-Flowers as a Highly Selective Catalyst for Electrochemical Reduction of CO_2 to Formate. *J. Electrochem. Soc.* **2018**, *165*, H594–H600. [CrossRef]
17. Wang, H.; Tang, C.; Sun, B.; Liu, J.; Xia, Y.; Li, W.; Jiang, C.; He, D.; Xiao, X. In-Situ Structural Evolution of Bi_2O_3 Nanoparticle Catalysts for CO_2 Electroreduction. *Int. J. Extrem. Manuf.* **2022**, *4*, 035002. [CrossRef]
18. Zelocualtecatl Montiel, I.; Dutta, A.; Kiran, K.; Rieder, A.; Iarchuk, A.; Vesztergom, S.; Mirolo, M.; Martens, I.; Drnec, J.; Broekmann, P. *CO_2 Conversion at High Current Densities: Stabilization of Bi(III) Containing Electrocatalysts under CO_2 Gas Flow Conditions*; American Chemical Society: Washington, DC, USA, 2022.

19. Xia, D.; Yu, H.; Xie, H.; Huang, P.; Menzel, R.; Titirici, M.M.; Chai, G. Recent Progress of Bi-Based Electrocatalysts for Electrocatalytic CO_2 Reduction. *Nanoscale* **2022**, *14*, 7957–7973. [CrossRef]
20. Medina-Ramos, J.; Dimeglio, J.L.; Rosenthal, J. Efficient Reduction of CO_2 to CO with High Current Density Using in Situ or Ex Situ Prepared Bi-Based Materials. *J. Am. Chem. Soc.* **2014**, *136*, 8361–8367. [CrossRef]
21. Burdyny, T.; Smith, W.A. CO2 Reduction on Gas-Diffusion Electrodes and Why Catalytic Performance Must Be Assessed at Commercially-Relevant Conditions. *Energy Environ. Sci.* **2019**, *12*, 1442–1453. [CrossRef]
22. Nguyen, T.N.; Dinh, C.T. Gas Diffusion Electrode Design for Electrochemical Carbon Dioxide Reduction. *Chem. Soc. Rev.* **2020**, *49*, 7488–7504. [CrossRef] [PubMed]
23. Yang, K.; Kas, R.; Smith, W.A.; Burdyny, T. Role of the Carbon-Based Gas Diffusion Layer on Flooding in a Gas Diffusion Electrode Cell for Electrochemical CO2 Reduction. *ACS Energy Lett.* **2021**, *6*, 33–40. [CrossRef]
24. Junge Puring, K.; Siegmund, D.; Timm, J.; Möllenbruck, F.; Schemme, S.; Marschall, R.; Apfel, U.P. Electrochemical CO_2 Reduction: Tailoring Catalyst Layers in Gas Diffusion Electrodes. *Adv. Sustain. Syst.* **2021**, *5*, 2000088. [CrossRef]
25. De Gregorio, G.L.; Burdyny, T.; Loiudice, A.; Iyengar, P.; Smith, W.A.; Buonsanti, R. Facet-Dependent Selectivity of Cu Catalysts in Electrochemical CO_2 Reduction at Commercially Viable Current Densities. *ACS Catal.* **2020**, *10*, 4854–4862. [CrossRef]
26. Sen, S.; Brown, S.M.; Leonard, M.; Brushett, F.R. Electroreduction of Carbon Dioxide to Formate at High Current Densities Using Tin and Tin Oxide Gas Diffusion Electrodes. *J. Appl. Electrochem.* **2019**, *49*, 917–928. [CrossRef]
27. Li, M.; Idros, M.N.; Wu, Y.; Garg, S.; Gao, S.; Lin, R.; Rabiee, H.; Li, Z.; Ge, L.; Rufford, T.E.; et al. Unveiling the Effects of Dimensionality of Tin Oxide-Derived Catalysts on CO_2 Reduction by Using Gas-Diffusion Electrodes. *React. Chem. Eng.* **2021**, *6*, 345–352. [CrossRef]
28. Del Castillo, A.; Alvarez-Guerra, M.; Solla-Gullón, J.; Sáez, A.; Montiel, V.; Irabien, A. Sn Nanoparticles on Gas Diffusion Electrodes: Synthesis, Characterization and Use for Continuous CO_2 Electroreduction to Formate. *J. CO2 Util.* **2017**, *18*, 222–228. [CrossRef]
29. Löwe, A.; Rieg, C.; Hierlemann, T.; Salas, N.; Kopljar, D.; Wagner, N.; Klemm, E. Influence of Temperature on the Performance of Gas Diffusion Electrodes in the CO_2 Reduction Reaction. *ChemElectroChem* **2019**, *6*, 4497–4506. [CrossRef]
30. Manolova, M.; Freudenberger, R.; Hildebrand, J.; Klemm, E.; Bienen, F.; Kopljar, D.; Wagner, N. Sn Electrodeposition on Gas Diffusion Electrodes for the Electrochemical CO2 Reduction. In Proceedings of the 14th European SOFC & SOE Forum 2020, Lucerne, Switzerland, 20–23 October 2020. [CrossRef]
31. Liu, J.; Li, P.; Bi, J.; Zhu, Q.; Han, B. Design and Preparation of Electrocatalysts by Electrodeposition for CO_2 Reduction. *Chem.—Eur. J.* **2022**, *28*, e202200242. [CrossRef]
32. Puippe, J.-C.; Leaman, F.; American Electroplaters and Surface Finishers Society. *Theory and Practice of Pulse Plating*; American Electroplaters and Surface Finishers Society: Orlando, FL, USA, 1986; ISBN 978-0-936569-02-4.
33. Shah, S.S.A.; Sufyan Javed, M.; Najam, T.; Molochas, C.; Khan, N.A.; Nazir, M.A.; Xu, M.; Tsiakaras, P.; Bao, S.-J. Metal Oxides for the Electrocatalytic Reduction of Carbon Dioxide: Mechanism of Active Sites, Composites, Interface and Defect Engineering Strategies. *Coord. Chem. Rev.* **2022**, *471*, 214716. [CrossRef]
34. Bienen, F.; Löwe, A.; Hildebrand, J.; Hertle, S.; Schonvogel, D.; Kopljar, D.; Wagner, N.; Klemm, E.; Andreas Friedrich, K. Degradation Study on Tin- and Bismuth-Based Gas-Diffusion Electrodes during Electrochemical CO_2 Reduction in Highly Alkaline Media. *J. Energy Chem.* **2021**, *62*, 367–376. [CrossRef]
35. Bienen, F.; Hildebrand, J.; Kopljar, D.; Wagner, N.; Klemm, E.; Friedrich, K.A. Importance of Time-Dependent Wetting Behavior of Gas-Diffusion Electrodes for Reactivity Determination. *Chem. Ing. Tech.* **2021**, *93*, 1015–1019. [CrossRef]
36. Löwe, A.; Schmidt, M.; Bienen, F.; Kopljar, D.; Wagner, N.; Klemm, E. Optimizing Reaction Conditions and Gas Diffusion Electrodes Applied in the CO_2 Reduction Reaction to Formate to Reach Current Densities up to 1.8 A Cm^{-2}. *ACS Sustain. Chem. Eng.* **2021**, *9*, 4213–4223. [CrossRef]
37. Kopljar, D.; Wagner, N.; Klemm, E. Transferring Electrochemical CO_2 Reduction from Semi-Batch into Continuous Operation Mode Using Gas Diffusion Electrodes. *Chem. Eng. Technol.* **2016**, *39*, 2042–2050. [CrossRef]
38. Alvarez-Guerra, M.; Quintanilla, S.; Irabien, A. Conversion of Carbon Dioxide into Formate Using a Continuous Electrochemical Reduction Process in a Lead Cathode. *Chem. Eng. J.* **2012**, *207–208*, 278–284. [CrossRef]
39. Alvarez-Guerra, M.; Del Castillo, A.; Irabien, A. Continuous Electrochemical Reduction of Carbon Dioxide into Formate Using a Tin Cathode: Comparison with Lead Cathode. *Chem. Eng. Res. Des.* **2014**, *92*, 692–701. [CrossRef]
40. Díaz-Sainz, G.; Alvarez-Guerra, M.; Solla-Gullón, J.; García-Cruz, L.; Montiel, V.; Irabien, A. CO_2 Electroreduction to Formate: Continuous Single-Pass Operation in a Filter-Press Reactor at High Current Densities Using Bi Gas Diffusion Electrodes. *J. CO2 Util.* **2019**, *34*, 12–19. [CrossRef]
41. Zhang, W.; Hu, Y.; Ma, L.; Zhu, G.; Zhao, P.; Xue, X.; Chen, R.; Yang, S.; Ma, J.; Liu, J.; et al. Liquid-Phase Exfoliated Ultrathin Bi Nanosheets: Uncovering the Origins of Enhanced Electrocatalytic CO_2 Reduction on Two-Dimensional Metal Nanostructure. *Nano Energy* **2018**, *53*, 808–816. [CrossRef]
42. Lu, P.; Gao, D.; He, H.; Wang, Q.; Liu, Z.; Dipazir, S.; Yuan, M.; Zu, W.; Zhang, G. Facile Synthesis of a Bismuth Nanostructure with Enhanced Selectivity for Electrochemical Conversion of CO_2 to Formate. *Nanoscale* **2019**, *11*, 7805–7812. [CrossRef]
43. Huang, J.; Guo, X.; Yang, J.; Wang, L. Electrodeposited Bi Dendrites/2D Black Phosphorus Nanosheets Composite Used for Boosting Formic Acid Production from CO_2 Electroreduction. *J. CO2 Util.* **2020**, *38*, 32–38. [CrossRef]

44. Koh, J.H.; Won, D.H.; Eom, T.; Kim, N.-K.; Jung, K.D.; Kim, H.; Hwang, Y.J.; Min, B.K. Facile CO_2 Electro-Reduction to Formate via Oxygen Bidentate Intermediate Stabilized by High-Index Planes of Bi Dendrite Catalyst. *ACS Catal.* **2017**, *7*, 5071–5077. [CrossRef]
45. Li, J.; Li, J.; Liu, X.; Chen, J.; Tian, P.; Dai, S.; Zhu, M.; Han, Y.-F. Probing the Role of Surface Hydroxyls for Bi, Sn and In Catalysts during CO_2 Reduction. *Appl. Catal. B Environ.* **2021**, *298*, 120581. [CrossRef]
46. Li, H.; Yue, X.; Qiu, Y.; Xiao, Z.; Yu, X.; Xue, C.; Xiang, J. Selective Electroreduction of CO_2 to Formate over the Co-Electrodeposited Cu/Sn Bimetallic Catalyst. *Mater. Today Energy* **2021**, *21*, 100797. [CrossRef]
47. Lv, W.; Zhou, J.; Bei, J.; Zhang, R.; Wang, L.; Xu, Q.; Wang, W. Electrodeposition of Nano-Sized Bismuth on Copper Foil as Electrocatalyst for Reduction of CO_2 to Formate. *Appl. Surf. Sci.* **2017**, *393*, 191–196. [CrossRef]
48. Pan, J.; Li, P.; Jiang, X.; Shen, Y.; Wang, M. Electrochemical CO_2 Reduction on Few-Atomic-Layer Bismuth Nanosheets. *Mater. Today Phys.* **2023**, *35*, 101096. [CrossRef]
49. Li, L.; Cai, F.; Qi, F.; Ma, D.-K. Cu Nanowire Bridged Bi Nanosheet Arrays for Efficient Electrochemical CO_2 Reduction toward Formate. *J. Alloy. Compd.* **2020**, *841*, 155789. [CrossRef]
50. Dutta, A.; Zelocualtecatl Montiel, I.; Kiran, K.; Rieder, A.; Grozovski, V.; Gut, L.; Broekmann, P. A Tandem ($Bi_2O_3 \rightarrow Bi_{met}$) Catalyst for Highly Efficient *Ec* -CO_2 Conversion into Formate: *Operando* Raman Spectroscopic Evidence for a Reaction Pathway Change. *ACS Catal.* **2021**, *11*, 4988–5003. [CrossRef]
51. Rabiee, H.; Ge, L.; Zhang, X.; Hu, S.; Li, M.; Smart, S.; Zhu, Z.; Yuan, Z. Shape-Tuned Electrodeposition of Bismuth-Based Nanosheets on Flow-through Hollow Fiber Gas Diffusion Electrode for High-Efficiency CO_2 Reduction to Formate. *Appl. Catal. B Environ.* **2021**, *286*, 119945. [CrossRef]
52. Rabiee, H.; Zhang, X.; Ge, L.; Hu, S.; Li, M.; Smart, S.; Zhu, Z.; Yuan, Z. Tuning the Product Selectivity of the Cu Hollow Fiber Gas Diffusion Electrode for Efficient CO_2 Reduction to Formate by Controlled Surface Sn Electrodeposition. *ACS Appl. Mater. Interfaces* **2020**, *12*, 21670–21681. [CrossRef]
53. Liu, S.; Hu, B.; Zhao, J.; Jiang, W.; Feng, D.; Zhang, C.; Yao, W. Enhanced Electrocatalytic CO_2 Reduction of Bismuth Nanosheets with Introducing Surface Bismuth Subcarbonate. *Coatings* **2022**, *12*, 233. [CrossRef]
54. Liang, X.-D.; Tian, N.; Hu, S.-N.; Zhou, Z.-Y.; Sun, S.-G. Recent Advances of Bismuth-Based Electrocatalysts for CO_2 Reduction: Strategies, Mechanism and Applications. *Mater. Rep. Energy* **2023**, *3*, 100191. [CrossRef]
55. Setterfield-Price, B.M.; Dryfe, R.A.W. The Influence of Electrolyte Identity upon the Electro-Reduction of CO_2. *J. Electroanal. Chem.* **2014**, *730*, 48–58. [CrossRef]
56. Thorson, M.R.; Siil, K.I.; Kenis, P.J.A. Effect of Cations on the Electrochemical Conversion of CO_2 to CO. *J. Electrochem. Soc.* **2013**, *160*, F69–F74. [CrossRef]
57. König, M.; Vaes, J.; Klemm, E.; Pant, D. Solvents and Supporting Electrolytes in the Electrocatalytic Reduction of CO_2. *iScience* **2019**, *19*, 135–160. [CrossRef] [PubMed]
58. Díaz-Sainz, G.; Alvarez-Guerra, M.; Solla-Gullón, J.; García-Cruz, L.; Montiel, V.; Irabien, A. Gas–Liquid–Solid Reaction System for CO_2 Electroreduction to Formate without Using Supporting Electrolyte. *AIChE J.* **2020**, *66*, e16299. [CrossRef]
59. Rabiee, H.; Ge, L.; Zhao, J.; Zhang, X.; Li, M.; Hu, S.; Smart, S.; Rufford, T.E.; Zhu, Z.; Wang, H.; et al. Regulating the Reaction Zone of Electrochemical CO_2 Reduction on Gas-Diffusion Electrodes by Distinctive Hydrophilic-Hydrophobic Catalyst Layers. *Appl. Catal. B Environ.* **2022**, *310*, 121362. [CrossRef]
60. Leonard, M.E.; Orella, M.J.; Aiello, N.; Román-Leshkov, Y.; Forner-Cuenca, A.; Brushett, F.R. Flooded by Success: On the Role of Electrode Wettability in CO_2 Electrolyzers That Generate Liquid Products. *J. Electrochem. Soc.* **2020**, *167*, 124521. [CrossRef]
61. Nwabara, U.O.; Cofell, E.R.; Verma, S.; Negro, E.; Kenis, P.J.A. Durable Cathodes and Electrolyzers for the Efficient Aqueous Electrochemical Reduction of CO_2. *ChemSusChem* **2020**, *13*, 855–875. [CrossRef]
62. Nwabara, U.O.; Hernandez, A.D.; Henckel, D.A.; Chen, X.; Cofell, E.R.; de-Heer, M.P.; Verma, S.; Gewirth, A.A.; Kenis, P.J.A. Binder-Focused Approaches to Improve the Stability of Cathodes for CO_2 Electroreduction. *ACS Appl. Energy Mater.* **2021**, *4*, 5175–5186. [CrossRef]
63. Kim, B.; Hillman, F.; Ariyoshi, M.; Fujikawa, S.; Kenis, P.J.A. Effects of Composition of the Micro Porous Layer and the Substrate on Performance in the Electrochemical Reduction of CO_2 to CO. *J. Power Sources* **2016**, *312*, 192–198. [CrossRef]
64. Baumgartner, L.M.; Koopman, C.I.; Forner-Cuenca, A.; Vermaas, D.A. When Flooding Is Not Catastrophic–Woven Gas Diffusion Electrodes Enable Stable CO_2 Electrolysis. *ACS Appl. Energy Mater.* **2022**, *5*, 15125–15135. [CrossRef] [PubMed]
65. Merino-Garcia, I.; Alvarez-Guerra, E.; Albo, J.; Irabien, A. Electrochemical Membrane Reactors for the Utilisation of Carbon Dioxide. *Chem. Eng. J.* **2016**, *305*, 104–120. [CrossRef]
66. Oßkopp, M.; Löwe, A.; Lobo, C.M.S.; Baranyai, S.; Khoza, T.; Auinger, M.; Klemm, E. Producing Formic Acid at Low PH Values by Electrochemical CO_2 Reduction. *J. CO2 Util.* **2022**, *56*, 101823. [CrossRef]
67. Van Daele, K.; De Mot, B.; Pupo, M.; Daems, N.; Pant, D.; Kortlever, R.; Breugelmans, T. Sn-Based Electrocatalyst Stability: A Crucial Piece to the Puzzle for the Electrochemical CO_2 Reduction toward Formic Acid. *ACS Energy Lett.* **2021**, *6*, 4317–4327. [CrossRef]
68. Alfath, M.; Lee, C.W. Recent Advances in the Catalyst Design and Mass Transport Control for the Electrochemical Reduction of Carbon Dioxide to Formate. *Catalysts* **2020**, *10*, 859. [CrossRef]
69. Endrődi, B.; Bencsik, G.; Darvas, F.; Jones, R.; Rajeshwar, K.; Janáky, C. Continuous-Flow Electroreduction of Carbon Dioxide. *Prog. Energy Combust. Sci.* **2017**, *62*, 133–154. [CrossRef]

70. Garg, S.; Li, M.; Weber, A.Z.; Ge, L.; Li, L.; Rudolph, V.; Wang, G.; Rufford, T.E. Advances and Challenges in Electrochemical CO_2 Reduction Processes: An Engineering and Design Perspective Looking beyond New Catalyst Materials. *J. Mater. Chem. A* **2020**, *8*, 1511–1544. [CrossRef]
71. Perry, S.C.; Leung, P.; Wang, L.; Ponce de León, C. Developments on Carbon Dioxide Reduction: Their Promise, Achievements, and Challenges. *Curr. Opin. Electrochem.* **2020**, *20*, 88–98. [CrossRef]
72. De Mot, B.; Hereijgers, J.; Duarte, M.; Breugelmans, T. Influence of Flow and Pressure Distribution inside a Gas Diffusion Electrode on the Performance of a Flow-by CO_2 Electrolyzer. *Chem. Eng. J.* **2019**, *378*, 122224. [CrossRef]
73. Chen, Z.; Rodriguez, A.G.; Nunez, P.; van Houtven, D.; Pant, D.; Vaes, J. Experimental Investigation of Anion Exchange Membrane Water Electrolysis for a Tubular Microbial Electrosynthesis Cell Design. *Catal. Commun.* **2022**, *170*, 106502. [CrossRef]
74. Yang, H.; Kaczur, J.J.; Sajjad, S.D.; Masel, R.I. Performance and Long-Term Stability of CO_2 conversion to Formic Acid Using a Three-Compartment Electrolyzer Design. *J. CO2 Util.* **2020**, *42*, 101349. [CrossRef]
75. Schweiss, R.; Meiser, C.; Damjanovic, T.; Galbiati, I.; Haak, N. *SIGRACET® Gas Diffusion Layers for PEM Fuel Cells, Electrolyzers and Batteries (White Paper)*; SGL Group: Wiesbaden, Germany, 2016.
76. Li, M.; Idros, M.N.; Wu, Y.; Burdyny, T.; Garg, S.; Zhao, X.S.; Wang, G.; Rufford, T.E. The Role of Electrode Wettability in Electrochemical Reduction of Carbon Dioxide. *J. Mater. Chem. A* **2021**, *9*, 19369–19409. [CrossRef]
77. Bertin, E.; Garbarino, S.; Roy, C.; Kazemi, S.; Guay, D. Selective Electroreduction of CO_2 to Formate on Bi and Oxide-Derived Bi Films. *J. CO2 Util.* **2017**, *19*, 276–283. [CrossRef]
78. Pander, J.E.; Baruch, M.F.; Bocarsly, A.B. Probing the Mechanism of Aqueous CO_2 Reduction on Post-Transition-Metal Electrodes Using ATR-IR Spectroelectrochemistry. *ACS Catal.* **2016**, *6*, 7824–7833. [CrossRef]
79. Egetenmeyer, A.; Radev, I.; Durneata, D.; Baumgärtner, M.; Peinecke, V.; Natter, H.; Hempelmann, R. Pulse Electrodeposited Cathode Catalyst Layers for PEM Fuel Cells. *Int. J. Hydrogen Energy* **2017**, *42*, 13649–13660. [CrossRef]
80. Pourbaix, M. *Atlas of Electrochemical Equilibria*; National Association of Corrosion Engineers: Houston, TX, USA, 1966.